Amplitudes for the analysis of the decay $J/\psi \to K^+ K^- \pi^0$

Peng Guo,[1] Ryan Mitchell,[1] Matthew Shepherd,[1] and Adam P. Szczepaniak[1,2]

[1]*Physics Department, Indiana University, Bloomington, Indiana 47405, USA*
[2]*Center For Exploration of Energy and Matter, Indiana University, Bloomington, Indiana 47408, USA*
(Received 17 December 2011; published 13 March 2012)

We construct an analytical model for two-channel, two-body scattering amplitudes, and then apply it in the description of the three-body $J/\psi \to K^+ K^- \pi^0$ decay. In the construction of the partial wave amplitudes, we combine the low-energy resonance region with the Regge asymptotic behavior determined from direct two-body production. We find that resonance production in the $K\pi$ channel in J/ψ decays seems to differ from that observed in direct $K\pi$ production, while the mass distribution in the $K\bar{K}$ channel may be compatible.

I. INTRODUCTION

Meson spectroscopy has played an important role in developing phenomenology and gaining insights into QCD in the nonperturbative domain. In an amplitude analysis of experimental data it is necessary to explore all of the available theoretical constraints because the extraction of resonance parameters requires the analysis of partial waves outside of the kinematic range of experimental data. In particular, amplitudes describing the mass distribution of a two-body subsystem in a quarkonium decay may be different from those describing scattering of the same two particles. In this paper we focus on the isospin 1/2, 1 and spin-one, P-wave scattering amplitudes in the $\pi\pi$, $K\bar{K}$ and $K\pi$ channels, and compare the phase shift data with two-body mass distributions from the three-body $J/\psi \to K^+ K^- \pi^0$ decay. These amplitudes are dominated by the ground-state vector resonances $\rho(770)$ and $K^*(892)$ that are well established as quark-antiquark, QCD bound states that are weakly coupled to the meson-meson continuum. There is also strong experimental evidence for higher mass vector resonances, although precisely how many and to what extent these are related to QCD single-hadron states remains an open issue [1–5].

In Table I we list the masses of the lowest vector-meson states obtained from recent lattice QCD simulations [6] and the quark potential model [7], and compare them to the data compiled by the Particle Data Group (PDG) [8]. Below 2 GeV the PDG lists two excited isovector resonances, the $\rho'(1450)$ and $\rho''(1700)$, that could have the quark model assignments of $2S$ and $1D$, respectively. In the lattice simulations of [6], the average pion mass is approximately 400 MeV, which puts the ρ meson approximately 130 MeV above its measured mass. Shifting the vector-mesons masses from lattice computations down by 130 MeV puts the first excited state around 1600 MeV, which is $\sim$150 MeV higher than the measured mass of the $\rho'(1450)$. While a resonance in the 1600–1700 MeV mass range can be clearly inferred from the $\pi\pi$-scattering phase shift data [2], the experimental evidence for the $\rho'(1450)$ is

ambiguous [8]. The main motivation for the $\rho'(1450)$ comes from the need to accommodate data on 4π production [9,10]. To the best of our knowledge, however, there has been no comprehensive analysis of all available P-wave data, and the importance of the various inelastic channels, possibly even the dominant one $K\bar{K}$, is yet to be settled. For example, an alternative scenario that seems to be supported by the lattice results might be that the $2S$ and $1D$ states are above 1.6 GeV while any residual strength corresponding to the PDG $\rho'(1450)$ could be due to residual interactions between pions and/or inelastic channel effects.

The vector mesons discussed above can be produced in $J/\psi \to K\bar{K}\pi$ and 3π decays. In this paper we focus on the former; we studied the latter in Ref. [11]. The $J/\psi \to K\bar{K}\pi$ decay has been analyzed by the BESII Collaboration [12]. The Dalitz plot distribution of the $K^+ K^- \pi^0$ events has clearly visible sharp bands corresponding to the isospin-1/2, $K^{\pm*}(892)$, and weaker bands in the first excited K'^*-resonance region. The distribution is shown in Fig. 1. There is also a significant enhancement in the low $K^+ K^-$-invariant mass region. In the BESII analysis this broadband was associated with a new isovector P-wave resonance $X(1570)$, decaying to $K^+ K^-$ with the pole position at $(1576 - 409i)$ MeV seen through a strong destructive interference with the $\rho(1700)$. There have been several theoretical attempts to explain this result [13,14].

In this work we address the following questions. Can the broad enhancement in the low-mass $K\bar{K}$ channel be described by the P-wave $K\bar{K}$ amplitudes determined from phase shift analysis? And, more generally, can the Dalitz plot distribution of $K\bar{K}\pi$ events in the J/ψ decay be described in terms of $K\bar{K}$ and $K\pi$ amplitudes reconstructed from phase shift analysis? To do so, we use, and further develop (by incorporating asymptotic energy dependence), the P-wave $\pi\pi$ and $K\bar{K}$ amplitudes initially constructed in [11,15]. The amplitudes that we use have the correct analytical properties, satisfy two-body unitarity, and reproduce the known data on $\pi\pi$ scattering [2,16,17]. In [11] we successfully used these amplitudes

TABLE I. Masses of the first few lowest-lying vector meson resonances.

	$\rho(1^{--})$	$K^*(1^-)$
Lattice QCD [6]	0.90	0.95
	1.8	1.8
	...	...
Quark model [7]	$0.77(1^3S_1)$	$0.90(1^3S_1)$
	$1.45(2^3S_1)$	$1.58(2^3S_1)$
	$1.66(1^3D_1)$	$1.78(1^3D_1)$
	...	...
PDG [8]	0.775	0.895
	1.465	1.414
	1.720	1.717

to describe the $J/\psi \to \pi^+\pi^-\pi^0$ Dalitz distribution. In particular, we have found that since the $\rho''(1700)$ is quite inelastic [2], destructive interference with the virtual $J/\psi \to K\bar{K}\pi \to 3\pi$ process is important in reducing the Dalitz plot intensity in the ρ'' resonance region. We will investigate if it is possible that a similar phenomenon is in operation in the $K\bar{K}\pi$-final state and whether the virtual $J/\psi \to 3\pi \to K\bar{K}\pi$ decay may be responsible for the broad structure at low K^+K^--invariant mass.

This paper is organized as follows. The partial wave decomposition of the decay $J/\psi \to K^+K^-\pi^0$ is given in Sec. II. In Sec. III, we discuss our P-wave amplitudes and compare with the BESII data of Fig. 1. Ideally, the set of partial waves that are developed here could be used in a full Dalitz plot analysis, but this requires a full knowledge of experimental acceptances and resolutions. In this work we simply compare, qualitatively, a sample of Dalitz plot distributions generated from our amplitudes with the BESII result of Fig. 1. We include more details on the amplitude construction in the appendixes.
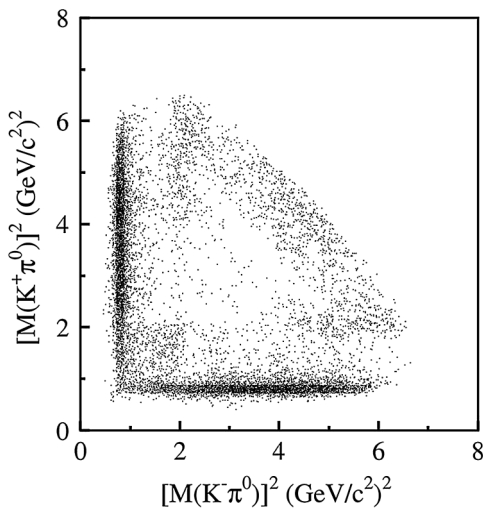
FIG. 1. The $J/\psi \to K^+K^-\pi^0$ Dalitz plot distribution from the BESII Collaboration [12].

II. PARTIAL WAVE AMPLITUDES IN THE $J/\psi \to K^+K^-\pi^0$ DECAY

Denoting the four momenta by $p_{\pm,0}$, P for $K^\pm$, π^0 and J/ψ, respectively, the general expression for the $J/\psi \to K^+K^-\pi^0$ amplitude is given by

$$\langle \pi^0 K^+ K^-, \text{out}|J/\psi(\lambda), \text{in}\rangle = i(2\pi)^4\delta^4\left(\sum_{i=0,\pm}p_i - P\right)T_\lambda.$$

(1)

The Dalitz plot invariants are defined by $s_{ij} = (p_i + p_j)^2$ with $i, j = \pm, 0$ referring to $K^\pm$ and the π^0, respectively. The general expression for the helicity amplitude of T_λ is given by

$$T_\lambda = \sum_{S,L}\sum_{\mu=\pm,0} N_{SL\mu}[D^{1*}_{\lambda,\mu}(r_{+-})d^S_{\mu,0}(\theta^+_{+-})F^{+-}_{SL}(s_{+-})$$
$$+ D^{1*}_{\lambda,\mu}(r_{+0})d^S_{\mu,0}(\theta^+_{+0})F^{+0}_{SL}(s_{+0})$$
$$+ D^{1*}_{\lambda,\mu}(r_{-0})d^S_{\mu,0}(\theta^-_{-0})F^{-0}_{SL}(s_{-0})],$$

(2)

where $N_{SL\mu} = \sqrt{3(2S+1)}\langle S\mu; L0|1\mu\rangle/4\pi$. Here λ is the spin projection of the J/ψ along the e^+e^- beam axis, which together with x and y define a lab coordinate system, S is the spin of a two-particle subsystem (the isobar), and L is the relative orbital angular momentum between the isobar and the spectator meson. The rotation r_{ij} is given by three Euler angles, $r_{ij} = r_{ij}(\phi_{ij}, \vartheta_{ij}, \psi^i_{ij})$, which rotate the standard configuration in the $(ij)k$-coupling scheme to the actual one. In the standard configuration of the $(ij)k$ coupling J/ψ is at rest, particle k has momentum along the negative z axis, and particles i and j have momenta in the xz plane with the particle j moving in the positive x direction. The azimuthal and polar angles, ϕ_{ij} and ϑ_{ij}, are defined in the J/ψ rest frame and refer to the actual direction of motion of the (ij) pair. Finally, ψ^i_{ij} and θ^i_{ij} are the azimuthal and the polar angle of the ith particle in the (ij) two-particle (isobar) rest frame.

The scalar form factors $F^{ij}_{SL}(s_{ij})$ describe the dynamics of the decay in the isobar model i.e. under the assumption that in a given isobar channel the form factors are functions of the subenergy of that isobar only. In the $L-S$ basis, the parity of the $K^+K^-\pi^0$ state is given by $P = (-1)^{S+L+1}$, and under charge conjugation the two isobar channels $|(K^+\pi^0)K^-\rangle$ and $|(K^-\pi^0)K^+\rangle$ are exchanged while the third isobar channel $|(K^+K^-)\pi^0\rangle$ is a charge-conjugation eigenstate with the eigenvalue $(-1)^S$. Thus, charge conjugation invariance implies that in Eq. (2) there are only two independent form factors, which we define as

$$F^{+-}_{SL} \equiv \frac{1-(-1)^S}{2}F^{K\bar{K}}_{SL}, \qquad F^{+0}_{SL} = -F^{-0}_{SL} \equiv -F^{K\pi}_{SL}$$

(3)

and obtain

$$T_\lambda = \sum_{S,L} \sum_{\mu=\pm1,0} N'_{SL\mu} [D^{1*}_{\lambda,\mu}(r_{+-}) d^S_{\mu,0}(\theta^+_{+-}) F^{+-}_{SL}(s_{+-})$$
$$- D^{1*}_{\lambda,\mu}(r_{+0}) d^S_{\mu,0}(\theta^+_{+0}) F^{K\pi}_{SL}(s_{+0})$$
$$+ D^{1*}_{\lambda,\mu}(r_{-0}) d^S_{\mu,0}(\theta^-_{-0}) F^{K\pi}_{SL}(s_{-0})] \qquad (4)$$

with $N'_{SL\mu} \equiv N_{SL\mu}(1 + (-1)^{S+L})/2$. The $\mu = 0$ component vanishes due to parity conservation, and we can further reduce the partial wave expansion to

$$T_\lambda = \sum_{S,L} N'_{SL1} \Big\{ [D^{1*}_{\lambda,1}(r_{+-})$$
$$+ D^{1*}_{\lambda,-1}(r_{+-})] d^S_{1,0}(\theta^+_{+-}) \frac{1-(-1)^S}{2} F^{K\bar{K}}_{SL}(s_{+-})$$
$$- [D^{1*}_{\lambda,1}(r_{+0}) + D^{1*}_{\lambda,-1}(r_{+0})] d^S_{1,0}(\theta^+_{+0}) F^{K\pi}_{SL}(s_{+0})$$
$$+ [D^{1*}_{\lambda,1}(r_{-0}) + D^{1*}_{\lambda,-1}(r_{-0})] d^S_{1,0}(\theta^-_{-0}) F^{K\pi}_{SL}(s_{-0}) \Big\}. \qquad (5)$$

Finally, it is useful to rewrite the above amplitude in terms of a single set of angles describing orientation of the decay plane. Using the relation between Euler rotations

$$r_{+-} = r_{-0} r(0, \chi_+, 0) = r_{+0} r^{-1}(0, 0, \pi) r^{-1}(0, \chi_-, 0), \qquad (6)$$

where $\chi_+(\chi_-)$ is the angle between K^+ (K^-) and π^0 and in the $K^+ K^- \pi^0$ rest frame, enables us to write T in terms of r_{+-} alone,

$$T_\lambda = \sum_{S,L} N'_{SL1} [D^{1*}_{\lambda,1}(r_{+-})$$
$$+ D^{1*}_{\lambda,-1}(r_{+-})] \Big[d^S_{1,0}(\theta^+_{+-}) \frac{1-(-1)^S}{2} F^{K\bar{K}}_{SL}(s_{+-})$$
$$+ d^S_{1,0}(\theta^+_{+0}) F^{K\pi}_{SL}(s_{+0}) + d^S_{1,0}(\theta^-_{-0}) F^{K\pi}_{SL}(s_{-0}) \Big]. \qquad (7)$$

The allowed quantum numbers in the $K^+ K^-$ channel are $S^{PC} = 1^{--}(\rho), 3^{--}(\rho_3), \ldots$, and in the $K^\pm \pi^0$ channels $S^P = 1^-(K^*), 2^+(K^*_2), 3^-(K^*_3), \ldots$. Throughout the rest of the paper we will assume that the Dalitz distribution can be saturated with the lowest partial waves, i.e. P waves in both $K^+ K^-$ and $K^\pm \pi^0$ channels, and we test this hypothesis by studying the effect of the D-wave resonances in the $K\pi$ channels. Parity conservation implies $S = L$; therefore, in the following we will simply denote F^{ij}_{SL} by F^{ij}_L. The (unnormalized) J/ψ partial-decay width with respect to one of the Dalitz invariants (e.g. $M_{K^+K^-} = \sqrt{s_{+-}}$) is obtained by integrating the square of the decay amplitude over the orientation of the decay plane and the other independent invariant

$$\frac{d\Gamma}{d\sqrt{s_{+-}}} = N\sqrt{s_{+-}} \int_{s^{dn}_{-0}(s_{+-})}^{s^{up}_{-0}(s_{+-})} ds_{-0} |T|^2 \qquad (8)$$

and

$$|T|^2 = \Bigg| \sum_{S,L} N'_{SL1} \Big[d^S_{1,0}(\theta^+_{+-}) \frac{1-(-1)^S}{2} F^{K\bar{K}}_L(s_{+-})$$
$$+ d^S_{1,0}(\theta^+_{+0}) F^{K\pi}_L(s_{+0}) + d^S_{1,0}(\theta^-_{-0}) F^{K\pi}_L(s_{-0}) \Big] \Bigg|^2. \qquad (9)$$

The overall normalization (N) is adjusted to match the measured number of events. It is $|T|^2$ that determines the distribution of events in the Dalitz plot (i.e. $|T|^2 = \text{const}$ would give a flat distribution). The integration limits $s^{up/dn}_{-0}(s_{+-})$ are roots of the equation, which define the boundary of the Dalitz plot

$$s_{+-} s_{+0} s_{-0} - (s_{+0} + s_{-0})(m^2_\pi m^2_K + M^2 m^2_K)$$
$$- s_{+-}(m^4_K + M^2 m^2_\pi)$$
$$+ 2(m^4_K m^2_\pi + M^2 m^4_K + 2M^2 m^2_K m^2_\pi) = 0. \qquad (10)$$

Projections along the $M_{K^+\pi} = \sqrt{s_{+0}}$ and $M_{K^-\pi} = \sqrt{s_{-0}}$ axes can be defined analogously.

In the following section we discuss parametrizations of the form factors $F^{K\bar{K}}_L$ and $F^{K\pi}_L$ in terms of two-body amplitudes. Any parameters remaining in these parametrizations, which are related to the production process as opposed to final-state interactions, should be determined by fitting the Dalitz distributions. As discussed in Sec. I we do not fit the published Dalitz distribution but instead show the predicted distributions for specific values of these parameters.

III. THEORETICAL MODEL FOR FORM FACTORS

Unitarity relates production form factors to two-body amplitudes. In [11,15] we constructed analytical representations for the isovector, P-wave, two-body, $\pi\pi$, and $K\bar{K}$ amplitudes. Here, we further extend the analysis of [11] by constraining the high-energy behavior and extending the approach to the $K\pi$ channel. We begin with a K matrix and phenomenological parametrization of the known data (on the real axis) on phase shifts and elasticities. Even though the K matrix offers an analytical representation for the amplitude, it often leads to spurious poles and zeros of the amplitude when extrapolated outside the physical region. Therefore, we use the analytical representation for phase shifts and inelasticity via the K matrix only in the data region and smoothly extrapolate to match the asymptotic behavior of the partial waves at high energies. We then use the amplitudes, constructed in this way, over the whole physical energy range as input into the Omnés-Muskhelishvili integral to construct the regular part of the scattering amplitude on the left-side of the complex s plane. With the $N(s)/D(s)$ representation, which is described below, we determine the amplitude over the entire s plane. Finally, we solve the unitarity relation for the form factors and write the J/ψ-decay amplitude in terms of the denominator functions $D(s)$ and production functions

$c_\alpha(s)$. In the following section, we describe these steps in a little more detail. All details of the amplitude construction are given in the Appendixes.

A. Amplitude parametrization

In [11] to describe the high energy limit of the isovector P wave, the following hypothesis was made: the S matrix is saturated by two channels, $\pi\pi$ and $K\bar{K}$, and the elastic-channel phase shifts asymptotically approach a multiple of π with elasticity η approaching 1. Even though J/ψ decays probe only a limited energy range, and are quite insensitive to details of the asymptotic behavior, we might as well use a different hypothesis that is better rooted in high energy phenomenology. It is known that at high energies, elastic cross sections slowly grow with energy almost approaching the Froissart bound. This implies that at an impact parameter larger than the interaction region $O(1\ \text{fm})$ there is no interaction while the low partial waves are suppressed, as if scattering from a "gray disk." The low partial waves correspond to $L \ll L_0(s)$ where $L_0(s) \sim \sqrt{s}/2$ fm, and while the interaction radius grows logarithmically with energy, the scattering of the low partial waves becomes logarithmically suppressed, i.e. $\eta_L \sim 1 - O(1/\log s)$. In the language of Regge exchanges, this picture corresponds to the Pomeron exchange at high energies. Furthermore, since asymptotically the number of inelastic channels grows rapidly, each individual inelastic amplitude, e.g. $\pi\pi \to K\bar{K}$, is expected to fall off with energy and is represented by exchange of nonvacuum quantum numbers, aka meson Regge trajectories. The hypothesis of two-channel dominance in the high energy limit is, therefore, not necessarily well justified. Throughout the rest of the paper, we adopt the Regge picture of high-energy scattering. Matching the K-matrix parametrization of the low-energy data with Regge asymptotics leads to amplitudes of the form (we drop the angular momentum label on the partial wave),

$$t_{\alpha,\beta}(s) = |t_{\alpha,\beta}(s)|e^{i\phi_{\alpha,\beta}(s)} = \begin{cases} t_{\alpha,\beta}^{K\,\text{matrix}}(s) & s < s_{\text{low}} \\ t_{\alpha\beta}^{\text{Regge}}(s) & s > s_{\text{high,}} \end{cases}$$

(11)

with $t_{\alpha,\beta}^{K\,\text{matrix}}(s)$ and $t_{\alpha\beta}^{\text{Regge}}(s)$ determined from K matrix fits to the low-energy data and Regge fits to the high-energy fixed t data, respectively. Greek indices denote two-body channels, i.e. $\alpha = (i, j) = \pi\pi$, $K\bar{K}$, etc. For energies between s_{low} and s_{high}, we smoothly connect both real and imaginary parts of the K matrix and Regge amplitudes. The denominator function in the N/D parametrization

$$t_{\alpha\beta}(s) = \frac{N_{\alpha\beta}(s)}{D_{\alpha\beta}(s)}$$

(12)

is then obtained from the phase of the scattering amplitude using the Omnés-Muskhelishvili solution of the unitarity

relation $[(s_{\text{th}} \gtrsim \min(s_\alpha, s_\beta)$, where s_α is the α-channel threshold]

$$\frac{\text{Im}D_{\alpha\beta}(s)}{D_{\alpha\beta}(s)} = -\sin\phi_{\alpha\beta}(s)e^{-2i\phi_{\alpha\beta}(s)}$$

(13)

and is given by

$$D_{\alpha\beta}(s) = e^{-(s/\pi)\int_{s_{\text{th}}}ds'\phi_{\alpha\beta}(s')/s'(s'-s)},$$

(14)

where we conveniently normalized $D_{\alpha\beta}(0) = 1$. The numerator functions $N_{\alpha\beta}(s)$ are given by the largely unknown discontinuity of the amplitudes on the left-hand cut. For the purpose of solving the unitarity relation for the J/ψ-decay form factors, which will be discussed below [cf. Eq. (16)], it is convenient to have $N_{\alpha\beta}(s)$'s for all intervening α, β channels having the same analytical form. This is certainly a simplifying approximation; nevertheless, we have found that with a simple parametrization

$$N_{\alpha\beta}(s) = \frac{\lambda_{\alpha\beta}}{s + s_L}$$

(15)

and with the two-body amplitudes given by Eqs. (12) and (14), it is indeed possible to obtain good fits to the two-body scattering data, i.e. phase shifts and elasticity.

Having constructed the two-body amplitudes, the next step is to relate them to the production form factors. This is done through the unitarity relations, which relate the imaginary part of the form factors to the two-body amplitudes

$$\text{Im}\,\hat{F}_L^\alpha(s) = \sum_\beta t_{\alpha,\beta}^*(s)\rho^\beta(s)\hat{F}_L^\beta(s)$$

(16)

with $\alpha\beta t$ representing the elastic L-partial wave scattering amplitude between two-body channels $\alpha = (ij)$ and $\beta = (i'j')$. $\hat{F}$ is the reduced form factor (with the barrier factor removed)

$$F_L^{ij}(s) = q_{ij}^L(s)p_k^L(s)\hat{F}_L^{ij}(s)$$

(17)

with $q_{ij}(s)$ being the relative momentum between mesons i and j,

$$q_{ij}(s) = \sqrt{\frac{[s - (m_i + m_j)^2][s - (m_i - m_j)^2]}{4s}}$$

(18)

and

$$p_k(s) = \sqrt{\frac{[s - (M + m_k)^2][s - (M - m_k)^2]}{4M^2}}$$

(19)

with M being the J/ψ mass, the relative momentum between the (ij) pair and the spectator meson k. $\rho_\alpha(s) = 2q_{ij}/\sqrt{s}$ describes the two-particle phase space. It is straightforward to show that if the scattering amplitude is dominated by a single resonance below inelastic threshold ($\rho = \rho^\alpha$, $\rho^\beta = 0$ for $\beta \neq \alpha$) the solution of the unitarity condition for $\hat{F}$ is

$$\hat{F}_L^{\alpha}(s) = c(s)\mathrm{BW}_R^L(s) = \frac{c(s)}{m_R^2 - s - im_R\Gamma_L(s)}, \quad (20)$$

where $\mathrm{BW}_R^L(s)$ is the Breit-Wigner amplitude [with an energy dependent width $\Gamma_L(s)$] and $c(s)$ is a real polynomial in s. In the general multiple-channel case, with the two-body amplitudes all parametrized by the same numerator function as in Eq. (15), the solution to Eq. (16) is given by [18]

$$\hat{F}^{\alpha}(s) = \sum_{\beta} \frac{c_{\beta}(s)}{D^{\alpha\beta}(s)} \quad (21)$$

with $c_{\beta}(s)$ being analytic functions in the right-hand plane and $\mathrm{Im}c_{\alpha}(s) = 0$ for $s > 0$.
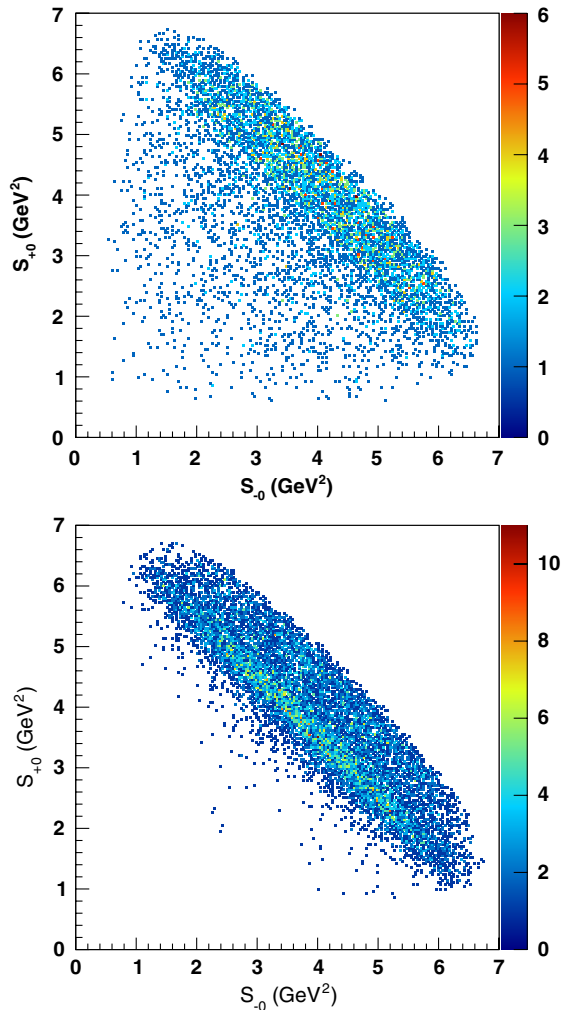
B. Results

As discussed in Sec. I, the original BESII analysis was based on the isobar, resonance parametrization of all three two-body channels. In the absence of a known isovector P-wave $K\bar{K}$ resonance to describe the low-mass $K\bar{K}$ enhancement, it was necessary to introduce a new resonance, the $X(1570)$. The $\pi\pi$-phase isovector P-wave shift data, however, points to significant inelasticity above 1.6 GeV, which following [2] we have attributed to the $K\bar{K}$ channel. The effect of the coupled $\pi\pi$ and $K\bar{K}$ channels on the $K^+K^-\pi^0$-mass distribution which follows from Eq. (21) is shown in Fig. 2.

In Fig. 3 we show the Dalitz distribution obtained using the single $K\pi$-channel amplitude (details are discussed in Appendix B). Besides the $K^*(892)$ peaks, bands at $M_{K\pi} = 1.75$ GeV are clearly visible in both $K^+\pi^0$ and $K^-\pi^0$-mass projections. These are due to the $K^*(1680)$ resonance clearly seen in the $K\pi$-phase shift analysis [19–21] but apparently not so in the $K\pi$ production from the J/ψ decay (cf. Fig. 1). This clear discrepancy indicates that it is not sufficient to use a single-channel $K\pi$ amplitude in the parametrization of the corresponding form factor in the J/ψ decay. As discussed in Appendix B, the $K\pi$ amplitude is indeed inelastic above $M_{K\pi} \sim$ 1.5 GeV with a possibility of a large coupling to the $K^*(892)\pi$ channel.

Finally, in Fig. 4 we show the Dalitz distribution obtained with a combination of three amplitudes, $K\bar{K} \to K\bar{K}$, $\pi\pi \to K\bar{K}$, and $K\pi \to K\pi$ with relative production coefficients $c_{\alpha}(s)$ chosen to best match the observed distribution in Fig. 1. While the low-mass $K\bar{K}$ region seems to be fairly well described, the resonance structures in the $K\pi$ channel do not match between the elastic $t_{K\pi \to K\pi}$ and J/ψ-decay amplitude. The $\pi\pi \to K\bar{K}$ and $K\bar{K} \to K\bar{K}$ amplitudes behave rather smoothly in the region corresponding to the $K\pi$ resonances and do not give enough

FIG. 2 (color online). Dalitz plot distribution obtained using, in Eq. (21), a single two-body $K\bar{K} \to K\bar{K}$ amplitude (top panel) and a single two-body $\pi\pi \to K\bar{K}$ amplitude (bottom panel) [i.e. with $c_{K\bar{K}} = 1$ ($c_{\pi\pi} = 1$) for the top (bottom) panel and $c_{\alpha}(s) = 0$ for all other waves].
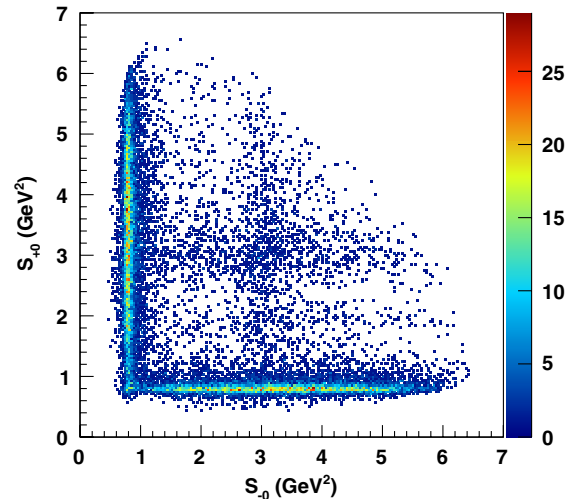

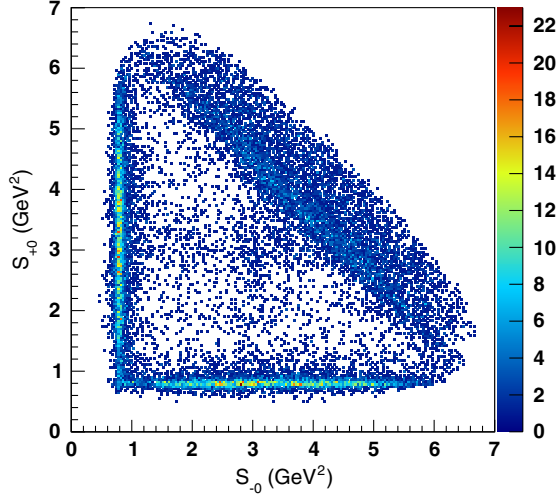FIG. 3 (color online). As in Fig. 2 but with a single two-body $K\pi \to K\pi$ amplitude.

FIG. 4 (color online). As in Fig. 2 but with three amplitudes $K\bar{K} \to K\bar{K}$, $\pi\pi \to K\bar{K}$, and $K\pi \to K\pi$ with relative production coefficients satisfying $c_{K\pi}(s): c_{K\bar{K}}(s): c_{\pi\pi}(s) = 1: 0.3: -0.7$.

strength to reduce the peak from the second K^*-resonance region. Thus, we anticipate that the discrepancy is due to inelasticities in the $K\pi$ channel itself. Since we are only comparing Dalitz distributions as opposed to fitting data, we do not attempt to further improve the comparison. It is worth noting that the $K^*(1410)$ listed in the PDG is indeed quite inelastic with only a 6.6% branching to $K\pi$.

IV. DISCUSSION AND CONCLUSION

Based on unitarity and analyticity we have constructed a set of analytical two-body amplitudes, which implement the known phase-shift data. These extend our previous work in coupled channel P-wave $\pi\pi$ and $K\bar{K}$ systems and the $J/\psi \to 3\pi$ decay [11]. The two-body amplitudes are only an approximation to the three-body decay; nevertheless, they provide a useful starting point and should match below-inelastic thresholds. We compared the analysis of the J/ψ decay with these amplitudes to the original analysis of the BESII Collaboration, which was based on the isobar model with coherent Breit-Wigner resonances. The isobar model with the known, low-mass resonances only and without inelasticities cannot faithfully produce the broad structure of low K^+K^--invariant mass, which is why in the BESII analysis an additional P-wave resonance $X(1576)$ coupled to K^+K^- was introduced. Our preliminary study indicates that the $K\bar{K}$ low-mass region may be described by the inelasticity in the $\pi\pi \to \pi\pi$ wave if attributed to the coupling between $\pi\pi$ and $K\bar{K}$ channels. A single $K\pi \to K\pi$ amplitude is strongly affected by the second vector $K^*(1680)$ resonance as observed in $K\pi$ phase-shift analysis. However, in J/ψ decay this resonance seems to be suppressed. It is worth noting that a similar suppression of the first excited isovector-vector resonance is also observed in the 3π decay of J/ψ [11].

APPENDIX A: ANALYTICAL MODEL FOR THE P-WAVE ISOVECTOR $\pi\pi \to \pi\pi$, $\pi\pi \to K\bar{K}$, AND $K\bar{K} \to K\bar{K}$ AMPLITUDES

1. K-matrix parametrization ($s < s_{\text{low}}$)

We use a two-channel K matrix [11] to fit the data on $\pi\pi \to \pi\pi$ P-wave phase shift and elasticity η from [2,16,17] (Figs. 5 and 6). With the S matrix saturated by two channels, the model makes a prediction for the phase shift in the $K\bar{K} \to K\bar{K}$ channel. In this section $\alpha, \beta = \pi$,
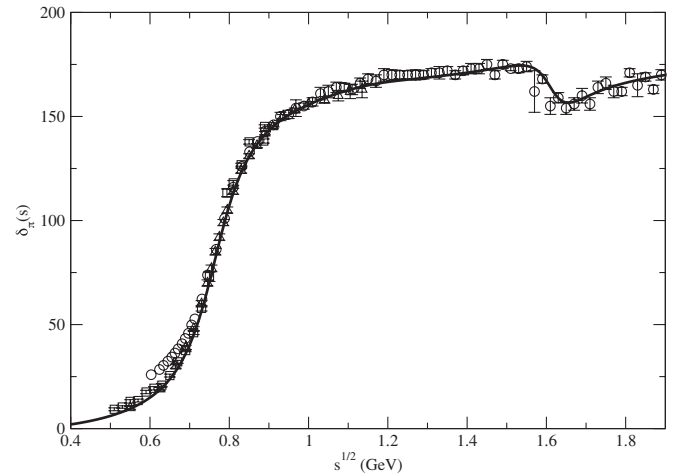

FIG. 5. Phase shift of the P-wave $\pi\pi$ amplitude. Data are taken from [2] (circles), [16] (triangles), and [17] (squares). The solid line is the result of the fit to δ_π and η with the analytical K-matrix representation described in the text.
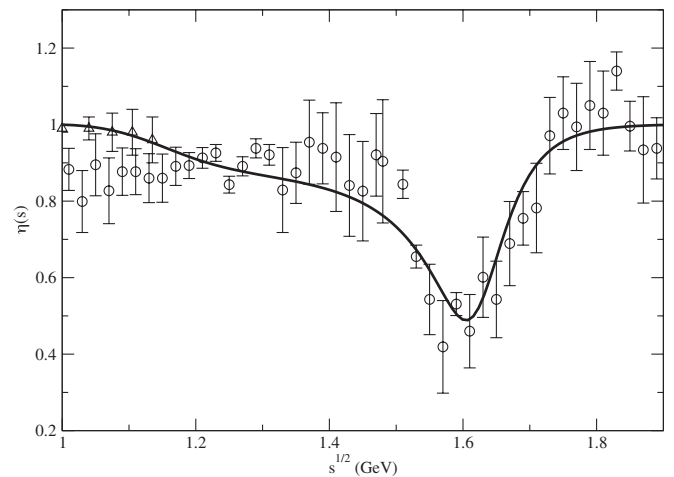

FIG. 6. Same as in Fig. 5 for the inelasticity η.

K correspond to the two-body channels $\pi\pi$ and $K\bar{K}$, respectively. The two-channel K-matrix representation is given by

$$[\hat{t}^{-1}(s)]_{\alpha\beta} = [K^{-1}(s)]_{\alpha\beta} + \delta_{\alpha\beta}(s - s_\alpha)I_\alpha(s), \quad (A1)$$

where

$$I_\alpha(s) = I_\alpha(0) - \frac{s}{\pi} \int_{s_\alpha}^\infty ds' \sqrt{1 - \frac{s_\alpha}{s'}} \frac{1}{(s' - s)s'}. \quad (A2)$$

A convenient choice for the subtraction constant $I_\alpha(0)$ is to take $\mathrm{Re}I_\alpha(M_\rho^2) = 0$ so that one of the poles of $K_{\pi\pi}$ corresponds to the Breit-Wigner mass squared $M_\rho^2 = (0.77 \text{ GeV})^2$ of the ρ meson. Using the general two-pole parametrization of the K matrix

$$K_{\pi\pi} = \frac{\alpha_\pi^2}{M_\rho^2 - s} + \frac{\beta_\pi^2}{s_2 - s} + \gamma_{\pi\pi},$$

$$K_{KK} = \frac{\beta_K^2}{s_2 - s} + \gamma_{KK}, \quad (A3)$$

$$K_{\pi K} = K_{K\pi} = \frac{\beta_\pi \beta_K}{s_2 - s} + \gamma_{\pi K},$$

where $\alpha_\pi^2 = \Gamma_\rho M_\rho^2/(M_\rho^2 - s_\pi)^{3/2}$, and fitting the P-wave $\pi\pi$ phase shift δ_π and the elasticity η, we obtain $\Gamma_\rho = 0.140 \text{ GeV}$ and

$$\sqrt{s_2} = 1.4708 \text{ GeV}, \quad \beta_\pi = 0.199, \quad \beta_K = 0.899,$$
$$\gamma_{\pi\pi} = 5.62 \times 10^{-2}, \quad \gamma_{\pi K} = 0.104, \quad \gamma_{KK} = 1.525, \quad (A4)$$

with the γ's in units of GeV^{-2}. The comparison of the phase shift and the inelasticity obtained with this parametrization and with the data is shown in Figs. 5 and 6. To illustrate unphysical features of the K-matrix parametrization, we rewrite Eq. (A1) using the standard N/D representation for $\hat{t}_{\alpha\beta} = t_{\alpha\beta}/(4q_\alpha q_\beta)$. With the normalization $D_{\alpha\beta}(0) = 1$ we obtain

$$N_{\pi\pi}(s) = \lambda_{\pi\pi} \frac{s - z_{\pi\pi}}{(s - s_{L,1})(s - s_{L,2})},$$

$$D_{\pi\pi}(s) = \exp\left(-\frac{s}{\pi} \int_{s_\pi} ds' \frac{\phi_{\pi\pi}(s')}{s'(s' - s)}\right),$$

$$N_{\pi K}(s) = \frac{\lambda_{\pi K}}{(s - s_{L,1})(s - s_{L,2})},$$

$$D_{\pi K}(s) = \frac{s_{1,\pi K} s_{2,\pi K}}{(s - s_{1,\pi K})(s - s_{2,\pi K})}$$
$$\times \exp\left(-\frac{s}{\pi} \int_{s_\pi} ds' \frac{\phi_{\pi K}(s')}{s'(s' - s)}\right),$$

$$N_{KK}(s) = \lambda_{KK} \frac{s - z_{KK}}{(s - s_{L,1})(s - s_{L,2})},$$

$$D_{KK}(s) = \exp\left(-\frac{s}{\pi} \int_{s_\pi} ds' \frac{\phi_{KK}(s')}{s'(s' - s)}\right) \quad (A5)$$

with $\lambda_{\pi\pi} = 5.649$, $\lambda_{KK} = 2.271$, and $\lambda_{\pi K} = 3.048 \text{ GeV}^2$. In this K matrix model, the left-hand cut of N is reduced to two poles at $s_{L,1} = -13.87 \text{ GeV}^2$ and $s_{L,2} = -0.787 \text{ GeV}^2$, respectively. There are also first-order zeros in $N_{\alpha\beta}$ at $z_{\pi\pi} = -0.867 \text{ GeV}^2$ and $z_{KK} = -13.78 \text{ GeV}^2$. Above the $K\bar{K}$ threshold the phase of the inelastic amplitude $\phi_{\pi K}$ is given by $\phi_{\pi K} = \delta_\pi + \delta_K$. From the K matrix we find that, asymptotically, $\phi_{\pi K}(\infty) = 2\pi$, which corresponds to two CDD [22] poles: one at the ρ mass $s_{1,\pi K} = M_\rho^2$, and the other at $s_{2,\pi K} = s_2 + \beta_\pi \beta_K/\gamma_{\pi K} = 3.884 \text{ GeV}^2$. Thus, while the K-matrix parametrization faithfully reproduces the $\pi\pi$ phase shift and elasticity in the whole available energy range, from $\pi\pi$ threshold up to 1.9 GeV, extrapolation beyond this range is problematic. The rapid decrease of $\phi_{\pi\pi}$ around $s \sim 6 \text{ GeV}^2$ seems unphysical. In the $\pi\pi \to K\bar{K}$ channel, the two CDD poles at m_ρ^2 and $s_2 + \beta_\pi \beta_K/\gamma_{\pi K}$ are clearly an artifact of the pole parametrization of the K matrix. A CDD pole in the inelastic channel above threshold (cf. the pole at $s_{2,\pi K} = 3.884 \text{ GeV}^2$) leads to a discontinuity in a phase shift and is unphysical. It also implies vanishing inelasticity $\eta = 1$ at this energy. A pole between $\pi\pi$ and $K\bar{K}$ thresholds is admissible, e.g. the pole at $s_{1,\pi K} = m_\rho^2$, but its strict overlap with the ρ mass is also an artifact of the parametrization. Since the phase space available in J/ψ decay extends up to $s_{\pi\pi} \sim 9 \text{ GeV}^2$ we need to remove these unphysical features of the K-matrix amplitude. As discussed in Sec. III we do this by using the K-matrix amplitudes below s_{low}, and above s_{high} we will use Regge parametrization.

2. Regge parametrization ($s > s_{\text{high}}$)

Regge analysis of $\pi\pi \to \pi\pi$ scattering has been studied recently in [23–25], and here we use the results of [25]. Parameters in Regge amplitudes were constrained by analyzing NN, πN, and $\pi\pi$ scattering data. For completeness, we give the following relevant formulas:

(i) $\pi\pi \to \pi\pi$

Regge parametrization involves the Regge poles corresponding to t-channel exchange of the Pomeron (P), the P' [associated with the $f_2(1270)$ trajectory], and the ρ. The t-channel isospin amplitudes are given by

$$F_{\pi\pi}^{(I_t=0)}(t, s, u) = -\frac{1 + e^{-i\pi\alpha_P(t)}}{\sin\pi\alpha_P(t)} P(s, t)$$
$$- \frac{1 + e^{-i\pi\alpha_{P'}(t)}}{\sin\pi\alpha_{P'}(t)} P'(s, t), \quad (A6)$$

$$F_{\pi\pi}^{(I_t=1)}(t, s, u) = \frac{1 - e^{-i\pi\alpha_\rho(t)}}{\sin\pi\alpha_\rho(t)} \beta_\rho \frac{1 + \alpha_\rho(t)}{1 + \alpha_\rho(0)} [1 + d_\rho t]$$
$$\times e^{bt}(s/\hat{s})^{\alpha_\rho(t)}, \quad (A7)$$

$$\text{Im}\, F_{\pi\pi}^{(I_t=2)}(t,s,u) = \beta_2 e^{bt}(s/\hat{s})^{\alpha_\rho(t)+\alpha_\rho(0)-1}, \quad (A8)$$

where ($\hat{s} = 1$ GeV)

$$P(s,t) = \beta_P \alpha_P(t) \frac{1+\alpha_P(t)}{2} e^{bt}(s/\hat{s})^{\alpha_P(t)}, \quad (A9)$$

$$P'(s,t) = \beta_{P'} \frac{\alpha_{P'}(t)[1+\alpha_{P'}(t)]}{\alpha_{P'}(0)[1+\alpha_{P'}(0)]} e^{bt}(s/\hat{s})^{\alpha_{P'}(t)} \quad (A10)$$

and the trajectories are given by

$$\alpha_P(t) = \alpha_P(0) + t\alpha'_P,$$
$$\alpha_{P'}(t) = \alpha_\rho(t) = \alpha_\rho(0) + t\alpha'_\rho + \frac{1}{2}t^2\alpha''_\rho. \quad (A11)$$

Numerical values of all parameters are given in Eqs. (B5), (B6) of [25]. The s-channel isospin, partial wave amplitudes are normalized according to

$$F_{\alpha,\beta}^{(I_s)}(s,t,u) = (\sqrt{2})^\sigma \frac{4}{\pi} \sum_L (2L+1) t_{\alpha,\beta}^{(LI_s)}(s) P_L(\cos\theta), \quad (A12)$$

where $(\sqrt{2})^\sigma$ is the identical particle symmetry factor: $\sigma = 2$ for $\pi\pi \leftrightarrow \pi\pi$, $\sigma = 1$ for $\pi\pi \leftrightarrow K\bar{K}$, and $\sigma = 0$ for $K\bar{K} \leftrightarrow K\bar{K}$. The s-channel amplitudes with $I_s = 0, 2$ are symmetric under $t \leftrightarrow u$ exchange; the $I_s = 1$ amplitude is antisymmetric and $s \leftrightarrow t$ crossing leads to the following relation between the s and the t-channel isospin amplitudes

$$F_{\pi\pi}^{(I_s=1)}(s,t,u) = \frac{1}{3}F_{\pi\pi}^{(I_t=0)}(t,s,u) + \frac{1}{2}F_{\pi\pi}^{(I_t=1)}(t,s,u)$$
$$- \frac{5}{6}F_{\pi\pi}^{(I_t=2)}(t,s,u) - (t \to u). \quad (A13)$$

The ($t \leftrightarrow u$) exchange brings in the u-channel Regge poles (these were ignored in [25] where only the forward $t = 0$ limit was considered). Finally, projecting out the P-wave amplitude yields

$$t_{\pi\pi}^{\text{Regge}}(s) = \frac{\pi}{16} \int_{-1}^{1} (d\cos\theta) \cos\theta \left[\frac{1}{3}F_{\pi\pi}^{(I_t=0)}(t,s,u) \right.$$
$$+ \frac{1}{2}F_{\pi\pi}^{(I_t=1)}(t,s,u) - \frac{5}{6}F_{\pi\pi}^{(I_t=2)}(t,s,u)$$
$$\left. - (t \to u) \right]. \quad (A14)$$

The angular integration is done numerically. The leading asymptotic behavior due to Pomeron exchange can be calculated analytically and is given by

$$t_{\pi\pi}^{\text{Regge}}(s) \simeq i \frac{\pi}{16} \frac{1}{3} \int_{-1}^{1} (d\cos\theta) \cos\theta [P(s,t) - P(s,u)]$$
$$\simeq i \frac{\pi}{24} \beta_P \frac{-3\alpha'_P + 2(b + \alpha'_P \ln s)}{(b + \alpha'_P \ln s)^2} s^{\alpha_P(0)-1}. \quad (A15)$$

To combine the K matrix ($s < s_{\text{low}}$) with the Regge projected ($s > s_{\text{high}}$) amplitudes into the full P-wave $\pi\pi \to \pi\pi$ amplitude

$$t_{\pi\pi}(s) = \begin{cases} t_{\pi\pi}^{K\,\text{matrix}}(s) & s < s_{\text{low}} \\ t_{\pi\pi}^{\text{Regge}}(s) & s > s_{\text{high}} \end{cases}, \quad (A16)$$

we choose $\sqrt{s_{\text{low}}} = 2.20$ GeV and $\sqrt{s_{\text{high}}} = 2.56$ GeV, and use a simple analytical formula to smoothly join the two amplitudes between s_{low} and s_{high}. The result is shown in Fig. 7.

(ii) $\pi\pi \to K\bar{K}$

Asymptotically the t-channel amplitude is dominated by the K^* trajectory

$$F_{\pi K}^{(I_t=(1/2))}(t,s,u) = \frac{1-e^{-i\pi\alpha_{K^*}(t)}}{\sin\pi\alpha_{K^*}(t)} \beta_{K^*} \frac{2\alpha_{K^*}(t)+1}{2\alpha_{K^*}(0)+1}$$
$$\times e^{bt}(\alpha'_{K^*}s)^{\alpha_{K^*}(t)}. \quad (A17)$$

Following [26] we use $b = 2.4$ GeV^{-2}, and $\alpha_{K^*}(t) = 0.352 + \alpha'_{K^*}t$ with $\alpha'_{K^*} = 0.882$ GeV^{-2}.
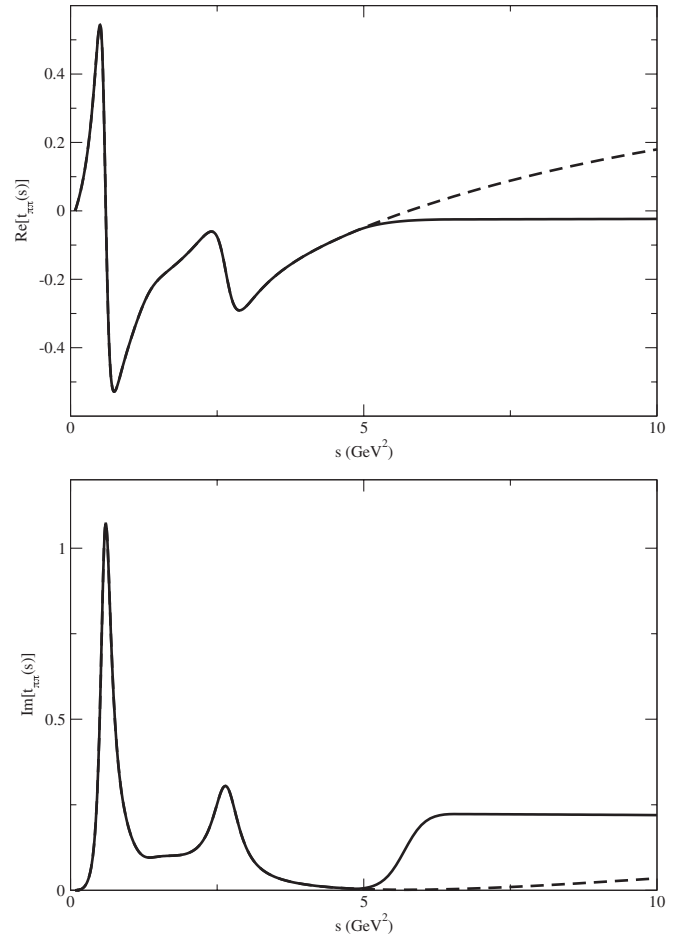

FIG. 7. Real (top panel) and imaginary (bottom panel) parts of the isovector, P-wave amplitude, $t_{\pi\pi}(s)$ (solid lines). The dashed line is the result of the K-matrix parametrization.

The s-channel $I_s = 1/2$ amplitude is antisymmetric under $t \leftrightarrow u$ exchange

$$F_{\pi K}^{(I_s=1)}(s, t, u) = -F_{\pi K}^{(I_s=1)}(s, u, t). \qquad \text{(A18)}$$

From $s \leftrightarrow t$ crossing we obtain

$$
\begin{aligned}
F_{\pi K}^{(I_s=1)}(s, t, u) = & \tfrac{2}{3} F_{\pi K}^{(I_t=(1/2))}(t, s, u) \\
& - \tfrac{2}{3} F_{\pi K}^{(I_t=(3/2))}(t, s, u) - (t \to u).
\end{aligned}
\qquad \text{(A19)}
$$

In terms of $F_{\pi K}^{(I_s=1)}(s, t, u)$, the properly normalized P wave in $\pi\pi \to K\bar{K}$ is finally given by

$$
\begin{aligned}
t_{\pi K}^{\text{Regge}}(s) = & \frac{\pi}{8\sqrt{2}} \int_{-1}^{1} (d\cos\theta) \\
& \times \cos\theta \left[\frac{2}{3} F_{\pi K}^{(I_t=(1/2))}(t, s, u) - (t \to u) \right].
\end{aligned}
\qquad \text{(A20)}
$$

We can fix β_{K^*} by matching our formula in Eq. (A17) to Eq. (81) in [26] in the limit of $t \to 0$ (forward direction). Taking into account differences in normalization employed here and used in [26], we find

$$
\begin{aligned}
\text{Im} F_{\pi K}^{(I_t=(1/2))} & (t, s, u)|_{s\to\infty, t\to 0} \\
& = \beta_{K^*} (\alpha'_{K^*} s)^{\alpha_{K^*}(0)} \\
& = \frac{3}{4\pi} \frac{\lambda}{\Gamma[\alpha_{K^*}(0)]} (\alpha'_{K^*} s)^{\alpha_{K^*}(0)}
\end{aligned}
\qquad \text{(A21)}
$$

with $\lambda = 1.82$ taken from [26] and

$$\beta_{K^*} = \frac{3}{4\pi} \frac{\lambda}{\Gamma[\alpha_{K^*}(0)]} = 0.172. \qquad \text{(A22)}$$

Asymptotically, $t_{\pi K}^{\text{Regge}}(s)$ approaches

$$
\begin{aligned}
t_{\pi K}^{\text{Regge}}(s) \simeq & \frac{1 - e^{-i\pi\alpha_{K^*}(0)}}{\sin\pi\alpha_{K^*}(0)} \beta_{K^*} \frac{\pi}{8\sqrt{2}} \frac{2}{3} \int_{-1}^{1} (d\cos\theta) \cos\theta \left[\frac{2\alpha_{K^*}(t) + 1}{2\alpha_{K^*}(0) + 1} e^{bt} (\alpha'_{K^*} s)^{\alpha_{K^*}(t)} - (t \to u) \right] \\
\simeq & \frac{1 - e^{-i\pi\alpha_{K^*}(0)}}{\sin\pi\alpha_{K^*}(0)} \frac{\pi}{3\sqrt{2}} \frac{\beta_{K^*} \alpha'_{K^*}}{2\alpha_{K^*}(0) + 1} \frac{(1 + 2\alpha_{K^*}(0))[b + \alpha'_{K^*} \ln(\alpha'_{K^*} s)] - 2\alpha'_{K^*}}{[b + \alpha'_{K^*} \ln(\alpha'_{K^*} s)]^2} (\alpha'_{K^*} s)^{\alpha_{K^*}(0)-1}.
\end{aligned}
\qquad \text{(A23)}
$$

The complete amplitude is given by

$$
t_{\pi K}(s) = \begin{cases} t_{\pi K}^{K \text{ matrix}}(s) & s < s_{\text{low}} \\ t_{\pi K}^{\text{Regge}}(s) & s > s_{\text{high}} \end{cases},
\qquad \text{(A24)}
$$

where we choose $\sqrt{s_{\text{low}}} = 2.5$ GeV and $\sqrt{s_{\text{high}}} = 3$ GeV as shown in Fig. 8.

(iii) $K\bar{K} \to K\bar{K}$

Asymptotically we only retain the Pomeron exchange

$$
\begin{aligned}
F_{K\bar{K}}^{(I_t=0)}(t, s, u) = & -\frac{1 + e^{-i\pi\alpha_P(t)}}{\sin\pi\alpha_P(t)} \beta_P^{K\bar{K}} \alpha_P(t) \\
& \times \frac{1 + \alpha_P(t)}{2} e^{bt} (s/\hat{s})^{\alpha_P(t)}
\end{aligned}
\qquad \text{(A25)}
$$

with $\alpha_P(t) = \alpha_P(0) + t\alpha'_P$ and all other parameters, except $\beta_P^{K\bar{K}}$, taken from [23,25], while for the Pomeron coupling to $K\bar{K}$ we use relation $\beta_P^{K\bar{K}} = \left(\frac{f_K^{(P)}}{f_\pi^{(P)}}\right)^2 (f_\pi^{(P)})^2 = 1.15$, where the values of $\frac{f_K^{(P)}}{f_\pi^{(P)}}$ and $\beta_P = (f_\pi^{(P)})^2$ are taken from [23,25]. From $s \leftrightarrow t$ crossing

$$
F_{K\bar{K}}^{(I_s=1)}(s, t, u) = \tfrac{1}{2} F_{K\bar{K}}^{(I_t=0)}(t, s, u) - \tfrac{1}{2} F_{K\bar{K}}^{(I_t=1)}(t, s, u).
\qquad \text{(A26)}
$$

For the Pomeron contribution to the s-channel P wave we thus find

$$
t_{K\bar{K}}^{\text{Regge}}(s) = \frac{\pi}{8} \int_{-1}^{1} (d\cos\theta) \cos\theta \frac{1}{2} F_{K\bar{K}}^{I_t=0}(t, s, u).
\qquad \text{(A27)}
$$

Asymptotically, $t_{K\bar{K}}^{\text{Regge}}(s)$ is given by

$$
\begin{aligned}
t_{K\bar{K}}^{\text{Regge}}(s) \simeq & i \frac{\pi}{16} \beta_P^{K\bar{K}} \int_{-1}^{1} (d\cos\theta) \cos\theta \alpha_P(t) \\
& \times \frac{1 + \alpha_P(t)}{2} e^{bt} s^{\alpha_P(t)} \\
\simeq & i \frac{\pi}{16} \beta_P^{K\bar{K}} \frac{-3\alpha'_P + 2(b + \alpha'_P \ln s)}{(b + \alpha'_P \ln s)^2} s^{\alpha_P(0)-1}.
\end{aligned}
\qquad \text{(A28)}
$$

In the full amplitude

$$
t_{K\bar{K}}(s) = \begin{cases} t_{K\bar{K}}^{K \text{ matrix}}(s) & s < s_{\text{low}} \\ t_{K\bar{K}}^{\text{Regge}}(s) & s > s_{\text{high}} \end{cases},
\qquad \text{(A29)}
$$

we take $\sqrt{s_{\text{low}}} = 1.62$ GeV and $\sqrt{s_{\text{high}}} = 3$ GeV for real parts of amplitudes and $\sqrt{s_{\text{low}}} = 1.64$ GeV and $\sqrt{s_{\text{high}}} = 1.8$ GeV for imaginary
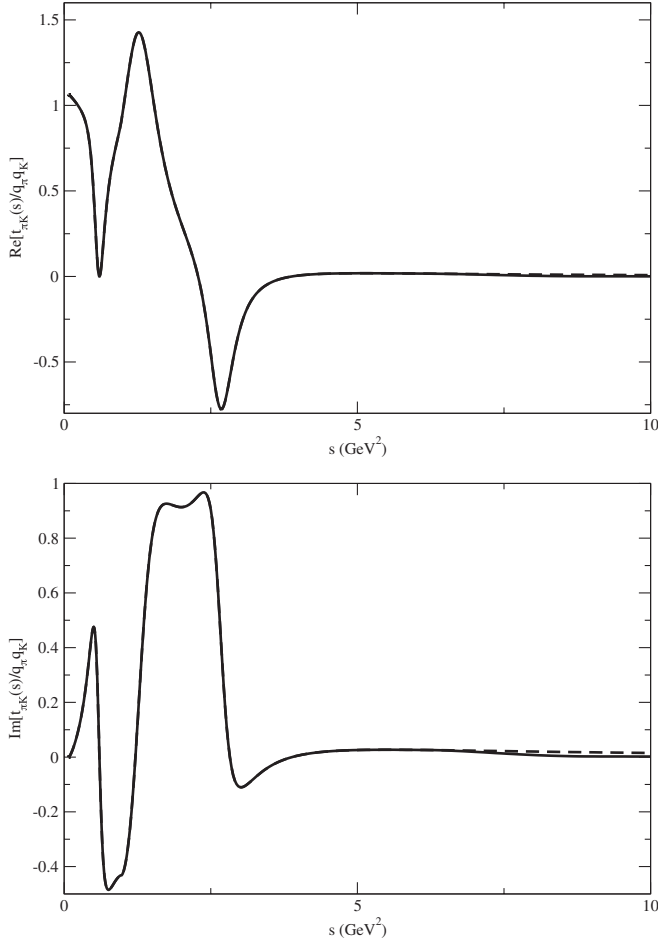
FIG. 8. Real (top panel) and imaginary (bottom panel) parts of the isovector, *P*-wave amplitude, $t_{\pi K}(s)/(q_\pi q_K)$ (solid lines). The dashed line is the result of the *K*-matrix parametrization.
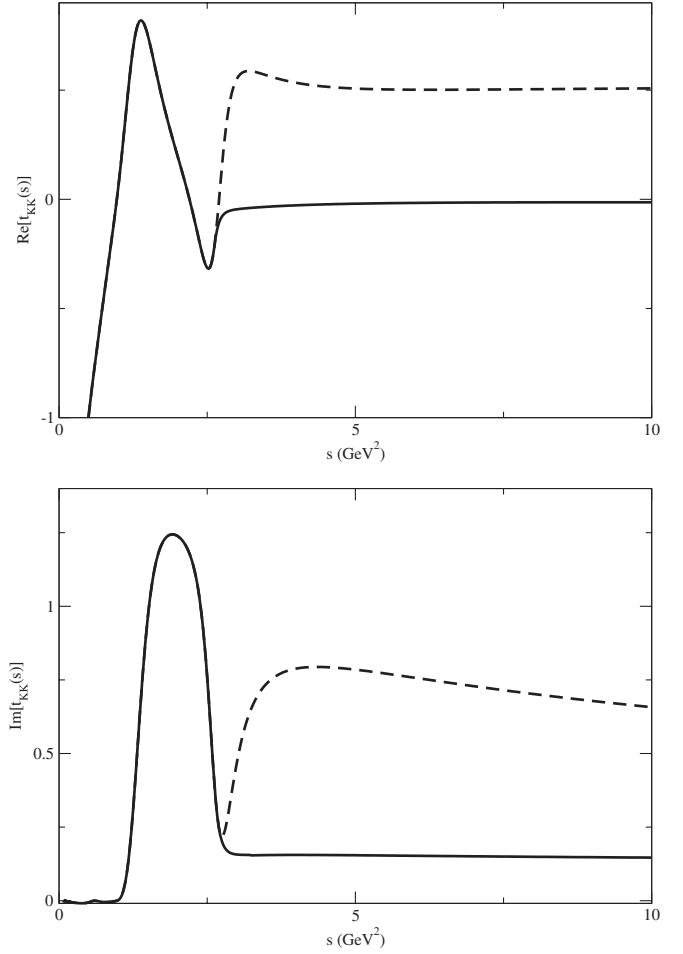

FIG. 9. Real (top panel) and imaginary (bottom panel) parts of the isovector, *P*-wave amplitude, $t_{K\bar{K}}(s)$ (solid lines). The dashed line is the result of the *K*-matrix parametrization.

parts of amplitudes. The different choice for the real and imaginary parts allows for a smoother connection with the Regge asymptotics. The phase of $t_{K\bar{K}}^{\mathrm{Regge}}(s)$ asymptotically approaches $\pi/2$, but the phase of $t_{K\bar{K}}^{K\,\mathrm{matrix}}(s)$ has a sharp drop above 1.65 GeV (see right plot in Fig. 10). Therefore, choosing $\sqrt{s_{\mathrm{low}}} \sim 1.64$ GeV allows for a continuous match between the phases of $t_{K\bar{K}}(s)$, as show in Fig. 9.

3. Phases of amplitudes and *D* functions

From Regge parametrizations, we find the following asymptotic behavior for the phases $\phi_{\alpha\beta}(s)$ of the complete amplitudes:

$$\phi_{\pi\pi} \to \arctan\left[-\frac{\sin\pi\alpha_P(0)}{1+\cos\pi\alpha_P(0)}\right] = \frac{\pi}{2}, \qquad (A30)$$

$$\phi_{\pi K} \to 2\pi + \arctan\left[\frac{\sin\pi\alpha_{K^*}(0)}{1-\cos\pi\alpha_{K^*}(0)}\right] \simeq 2\pi + \frac{\pi}{3}, \qquad (A31)$$

$$\phi_{K\bar{K}} \to \arctan\left[-\frac{\sin\pi\alpha_P(0)}{1+\cos\pi\alpha_P(0)}\right] = \frac{\pi}{2}. \qquad (A32)$$

These are shown in Fig. 10. For the *D* function, the Regge parametrization leads to the following asymptotic limits [cf. Eq. (14)]

$$\frac{1}{D_{\pi\pi}(s)} \to \frac{i}{s^{(1/2)}},$$

$$\frac{1}{D_{\pi K}(s)} \to \frac{1-e^{-i\pi\alpha_{K^*}(0)}}{\sin\pi\alpha_{K^*}(0)}\frac{1}{s^{2+(1/3)}}, \qquad (A33)$$

$$\frac{1}{D_{K\bar{K}}(s)} \to \frac{i}{s^{(1/2)}}.$$

APPENDIX B: ANALYTICAL MODEL FOR THE *P*-WAVE $\pi K \to \pi K$ AMPLITUDE

1. *K*-matrix parametrization ($s < s_{\mathrm{low}}$)

To fit the phase shift data on πK scattering, we use a two-channel *K* matrix model, with the two channels
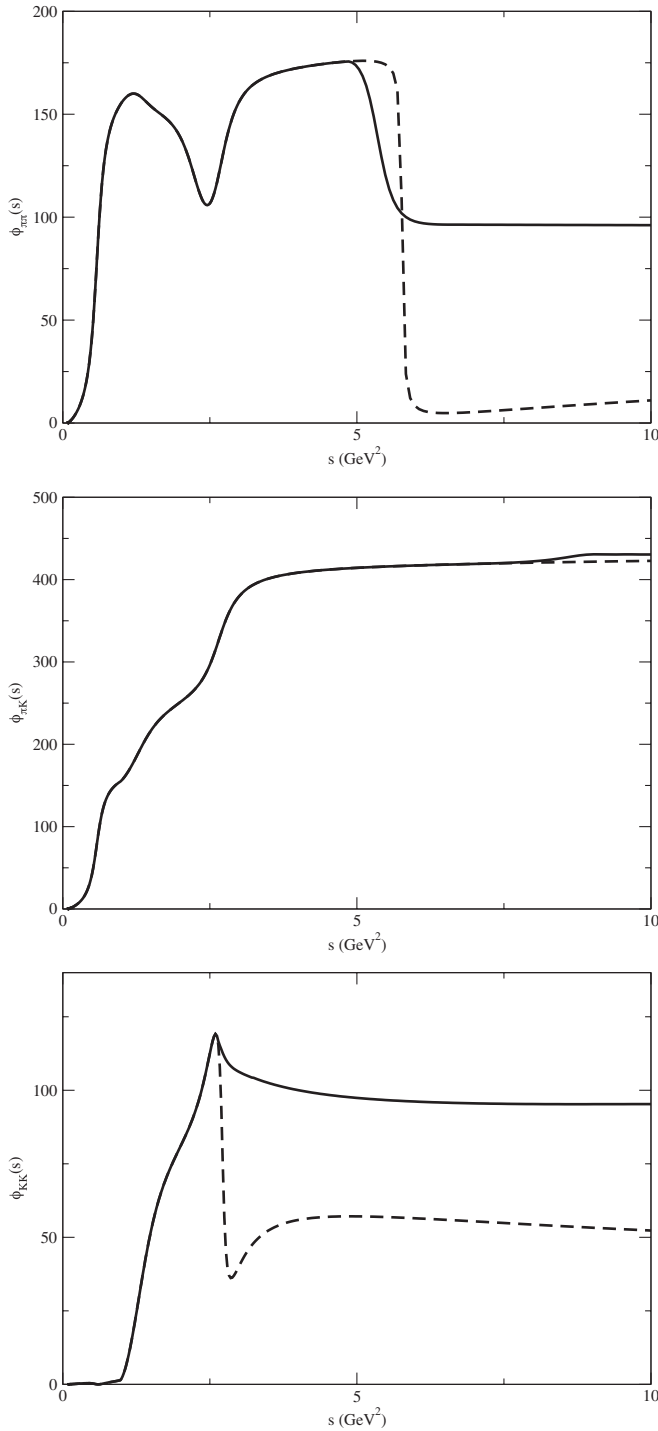
FIG. 10.   Phase of the $\pi\pi$ (top panel), πK (middle panel), and $K\bar{K}$ (bottom panel) P-wave amplitude. The dashed line is the result of the K-matrix parametrization from Eq. (5).

being $K\pi$ and $K^*(892)\pi$; in the second channel we treat K^* as a stable particle (i.e. we ignore cuts on the third sheet). Similarly to the $\pi\pi$, $K\bar{K}$ case for the K-matrix representation of $K\pi$ and $K^*(892)\pi$ amplitudes we write

$$[\hat{t}^{-1}(s)]_{\alpha\beta} = [K^{-1}(s)]_{\alpha\beta} + \delta_{\alpha\beta} \frac{(s - s_\alpha^+)(s - s_\alpha^-)}{s} I_\alpha(s),$$

$$\text{(B1)}$$

where $\hat{t}_{\alpha\beta} \equiv t_{\alpha\beta}/(4q_\alpha q_\beta)$,

$$q_\alpha = \sqrt{\frac{(s - s_\alpha^+)(s - s_\alpha^-)}{4s}}, \qquad s_\alpha^\pm = (m_\alpha \pm m_\pi)^2,$$

$$m_1 = m_K, \qquad m_2 = M_{K^*(892)}, \qquad \text{(B2)}$$

and

$$I_\alpha(s) = I_\alpha(0) - \frac{s}{\pi} \int_{s_\alpha^+}^\infty ds' \frac{\sqrt{(1 - \frac{s_\alpha^+}{s'})(1 - \frac{s_\alpha^-}{s'})}}{s'(s' - s)}. \quad \text{(B3)}$$

A convenient choice for the subtraction constant $I_\alpha(0)$ is to take $\text{Re}I_\alpha(M_{K^*(892)}^2) = 0$ so that one of the poles of K_{11} is located at mass squared of the $K^*(892)$, m_2^2. In terms of phase shift and inelasticity, the $K\pi$ and $K^*(892)\pi$ amplitudes are given by

$$t_{11} = \frac{\eta e^{2i\delta_{11}} - 1}{2i\rho_1}, \qquad t_{22} = \frac{\eta e^{2i\delta_{22}} - 1}{2i\rho_2},$$

$$t_{12} = t_{21} = \frac{\sqrt{1 - \eta^2} e^{i(\delta_{11} + \delta_{22})}}{2\sqrt{\rho_1 \rho_2}}, \qquad \text{(B4)}$$

where $\rho_\alpha(s) = \sqrt{(1 - \frac{s_\alpha^+}{s})(1 - \frac{s_\alpha^-}{s})}$. The denominators $D_{\alpha\beta}$ of the $K\pi$ and $K^*(892)\pi$ amplitudes are defined by the Omnés-Muskhelishvili function

$$D_{\alpha\beta}(s) = \exp\left(-\frac{s}{\pi} \int_{(m_K + m_\pi)^2}^\infty ds' \frac{\phi_{\alpha\beta}(s')}{s'(s' - s)}\right). \quad \text{(B5)}$$

To fit the P-wave phase shift data [19–21] we use a three-pole parametrization of the K matrix

$$K_{11} = \frac{\alpha_1^2}{M_{K^*(892)}^2 - s} + \frac{\beta_1^2}{s_2 - s} + \frac{\lambda_1^2}{s_3 - s} + \gamma_{11}^{(0)} + \gamma_{11}^{(1)}s,$$

$$K_{22} = \frac{\beta_2^2}{s_2 - s} + \frac{\lambda_2^2}{s_3 - s} + \gamma_{22}^{(0)} + \gamma_{22}^{(1)}s, \quad \text{(B6)}$$

$$K_{12} = K_{21} = \frac{\beta_1\beta_2}{s_2 - s} + \frac{\lambda_1\lambda_2}{s_3 - s} + \gamma_{12}^{(0)} + \gamma_{12}^{(1)}s,$$

where

$$\alpha_1^2 = \frac{\Gamma_{K^*(892)} M_{K^*(892)}^5}{[(M_{K^*(892)}^2 - s_1^+)(M_{K^*(892)}^2 - s_1^-)]^{3/2}}. \quad \text{(B7)}$$

And, for the parameters of the K matrix we obtain $\Gamma_{K^*(892)} = 0.0504$ GeV,
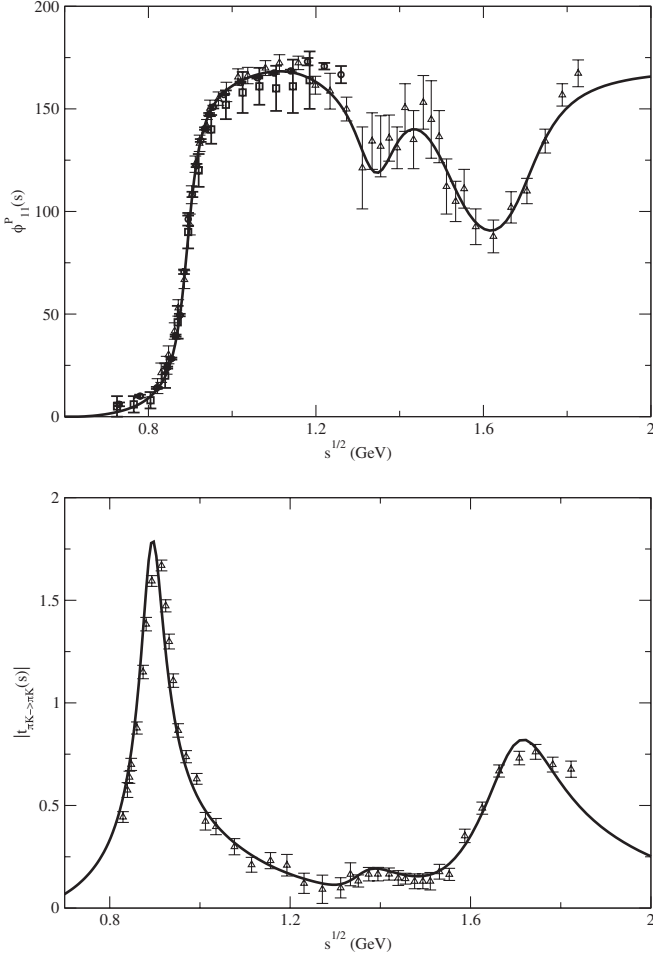
FIG. 11. ϕ_{11} (top panel) and $|t_{11}|$ (bottom panel) of $K\pi \to K\pi$ scattering amplitude vs data from [20] (squares), [21] (circles), and [19] (triangles).

$$\sqrt{s_2} = 1.35 \text{ GeV}, \qquad \sqrt{s_3} = 1.75 \text{ GeV},$$
$$\beta_1 = 0.110, \qquad \beta_2 = -0.685,$$
$$\lambda_1 = 0.142, \qquad \lambda_2 = 1.089.$$
$$\gamma_{11}^{(0)} = 0.204, \qquad \gamma_{12}^{(0)} = -0.983,$$
$$\gamma_{22}^{(0)} = 8.329, \qquad \gamma_{11}^{(1)} = -0.052, \qquad \text{(B8)}$$
$$\gamma_{12}^{(1)} = 0.426, \qquad \gamma_{22}^{(1)} = -3.834$$

with the $\gamma^{(0)}$'s in units of GeV^{-2} and $\gamma^{(1)}$'s in units of GeV^{-4}. The phase ϕ_{11} and magnitude $|t_{11}|$ of the $K\pi \to K\pi$-scattering amplitude is compared to the data in Fig. 11. We can express $\hat{t}_{\alpha\beta} = t_{\alpha\beta}/(4q_\alpha q_\beta)$ in

terms of a product of poles, zeros, and the Omnés-Muskhelishvili function

$$\hat{t}_{\alpha\beta} = N_{\alpha\beta} \frac{\prod_{l=1,N_{z,\alpha\beta}}(s - s_{z,l}^{(\alpha\beta)})}{\prod_{l=1,8}(s - s_{P,l})}$$
$$\times \exp\left(\frac{s}{\pi} \int_{(m_K+m_\pi)^2}^{\infty} ds' \frac{\phi_{\alpha\beta}(s')}{s'(s'-s)}\right), \quad \text{(B9)}$$

where $N_{z,\alpha\beta}$ is the number of zeros of $\hat{t}_{\alpha\beta}$ for which we find $N_{z,11} = N_{z,22} = 7$, $N_{z,12} = N_{z,21} = 6$. The normalization factors are given by $N_{11} = 7.075$, $N_{12} = -421.989$, $N_{22} = 2.808$. The positions of the poles and zeros are given by (in units of GeV^2)

$$s_{P,1/2} = 0.3573 \pm i0.4055,$$
$$s_{P,3/4} = 2.4912 \pm i0.5762,$$
$$s_{P,5/6} = 20.3504 \pm i3.3856, \qquad \text{(B10)}$$
$$s_{P,7} = -0.00489,$$
$$s_{P,8} = -6.2666,$$

and

$$s_{z,1/2}^{(11)} = 0.3428 \pm i0.4470,$$
$$s_{z,3/4}^{(11)} = 2.2188 \pm i0.6175,$$
$$s_{z,5/6}^{(11)} = 12.8061 \pm i0.2470,$$
$$s_{z,7}^{(11)} = 0. s_{z,1/2}^{(12)} = 1.9181 \pm i0.3669,$$
$$s_{z,3}^{(12)} = 3.3956, \qquad s_{z,4}^{(12)} = M_{K^*(892)}^2, \qquad \text{(B11)}$$
$$s_{z,5/6}^{(11)} = 0. \qquad s_{z,1/2}^{(22)} = 2.2704 \pm i0.2273,$$
$$s_{z,3/4}^{(22)} = 20.2775 \pm i3.3479, \qquad s_{z,5}^{(22)} = -0.00489,$$
$$s_{z,6}^{(22)} = -6.1874, \qquad s_{z,7}^{(22)} = 0,$$

respectively. As can be seen from Fig. 12, this K matrix leads to a dramatic, most likely unphysical, drop in the phase ϕ_{11} (dashed line) around 6 GeV^2 and results in both ϕ_{11} and δ_{11} vanishing asymptotically. Furthermore, the resulting t matrix has complex poles and zeros on the physical sheet [see Eqs. (B11) and (B11)]. The origin of these unphysical poles can be illustrated by considering a single channel K_{11} only, with a single pole and constant background term. The resulting t-matrix element is then given by
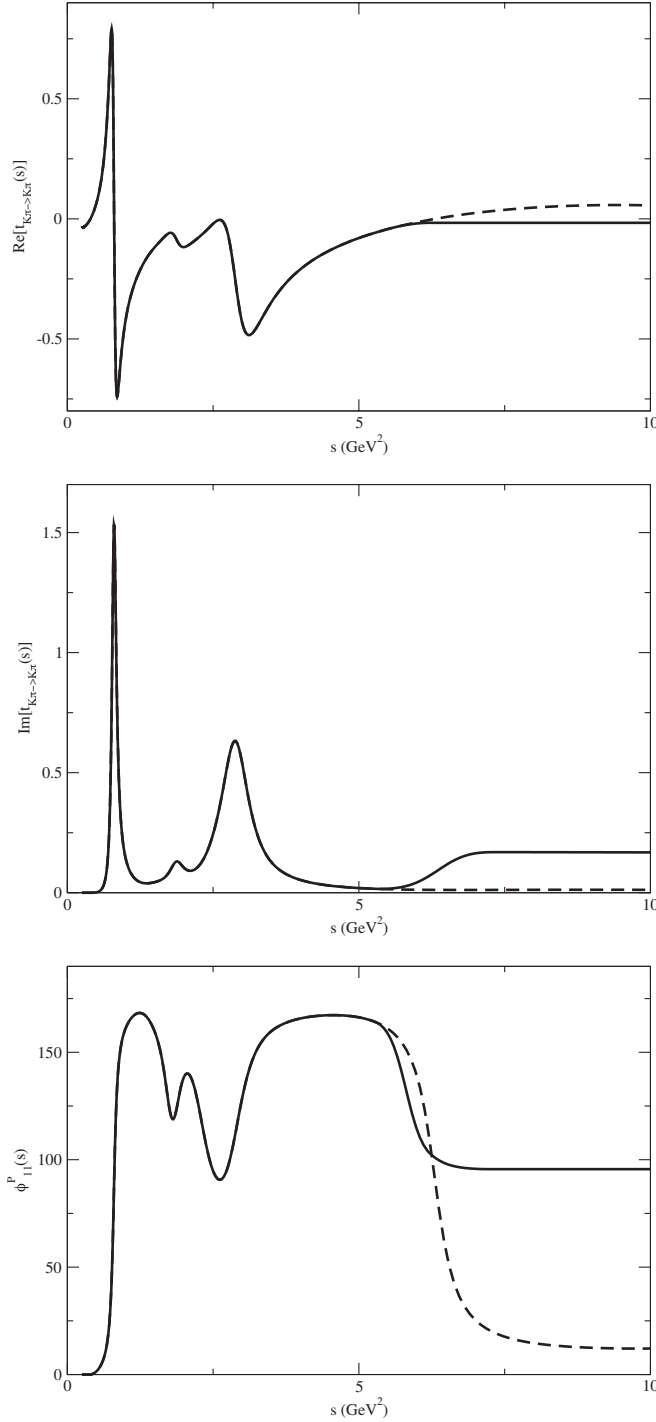
$$\hat{t}_{11} = \frac{1}{8} \frac{\alpha_1^2 + \gamma_{11}^0(M_{K^*(892)}^2 - s)}{(M_{K^*(892)}^2 - s) - \frac{[s-(m_K-m_\pi)^2][s-(m_K+m_\pi)^2]}{s} I_1(s)[\alpha_1^2 + \gamma_{11}^0(M_{K^*(892)}^2 - s)]}. \qquad \text{(B12)}$$

If, for simplicity, we replace m_K by m_π and keep only the imaginary of $I_1(s)$, in the limit $|s| \to \infty$ and $\gamma_{11}^0 \to 0$ with $|\gamma_{11}^0||s| \gg \alpha_1^2$ one finds

FIG. 12.   Real (top panel) and imaginary (middle panel) parts of the isovector, P-wave amplitude, $t_{\pi K \to \pi K}(s)$ and phase ϕ_{11} (solid curves). The dashed curves are the result of the K-matrix parametrization.

$$\hat{t}_{11} \to \frac{1}{8} \frac{\gamma_{11}^0}{1 - i\sqrt{1 - \frac{4m_\pi^2}{s}}\gamma_{11}^0 s}. \qquad (B13)$$

In the limit $\gamma_{11}^0 \to 0$ the pole is on the first sheet and approaches $s \to \pm \frac{i}{\gamma_{11}^0}$. Even though the K matrix itself

has unphysical singularities and zeros it still faithfully reproduces the phase and magnitude of the amplitude of $K\pi$-scattering data up to 1.8 GeV. Similarly to the cases in $\pi\pi$ and $K\bar{K}$ scattering presented in previous sections, we will truncate the K matrix solution at s_{low} and match it with Regge parametrization at s_{high}.

2. Regge parametrization for $\pi^0 K^\pm \to \pi^0 K^\pm$ ($s > s_{\text{high}}$)

Asymptotically we only retain the Pomeron (P) in the t channel and the K^* trajectory in the u channel

$$F_{\pi K \to \pi K}^{I_t=0}(t, s, u) = -\frac{1 + e^{-i\pi\alpha_P(t)}}{\sin\pi\alpha_P(t)} \beta_P^{\pi K} \alpha_P(t)$$
$$\times \frac{1 + \alpha_P(t)}{2} e^{bt}(s/\hat{s})^{\alpha_P(t)}, \qquad (B14)$$

$$F_{\pi K \to \pi K}^{I_u=(1/2)}(u, t, s) = \frac{1 - e^{-i\pi\alpha_{K^*}(u)}}{\sin\pi\alpha_{K^*}(u)} \beta_{K^*} \frac{2\alpha_{K^*}(u) + 1}{2\alpha_{K^*}(0) + 1}$$
$$\times e^{bu}(\alpha'_{K^*}s)^{\alpha_{K^*}(u)}. \qquad (B15)$$

The Pomeron trajectory is given in Eq. (A11) with parameters in Pomeron parametrization taken from [23,25], except for the coupling constant $\beta_P^{\pi K} = f_\pi^{(P)} f_K^{(P)} = [\beta_P^{\pi\pi} \beta_P^{K\bar{K}}]^{1/2} = 1.709$. The K^* trajectory is given by $\alpha_{K^*}(u) = 0.352 + 0.882u$ as in Appendix A. From s–t and s–u channel crossings, we obtain

$$F_{\pi K \to \pi K}^{I_s=(1/2)}(s, t, u) = \frac{1}{\sqrt{6}} F_{\pi K \to \pi K}^{I_t=0}(t, s, u) + F_{\pi K \to \pi K}^{I_t=1}(t, s, u)$$
$$+ \frac{1}{3} F_{\pi K \to \pi K}^{I_u=(1/2)}(u, t, s) + \frac{4}{3} F_{\pi K \to \pi K}^{I_u=(3/2)}(u, t, s). \qquad (B16)$$

The P-wave projection of the Regge amplitude in $\pi K \to \pi K$ scattering is given by

$$t_{\pi K \to \pi K}^{\text{Regge}}(s) = \frac{\pi}{8} \int_{-1}^{1} (d\cos)\cos\theta \left[\frac{1}{\sqrt{6}} F_{\pi K \to \pi K}^{I_t=0}(t, s, u) \right.$$
$$\left. + \frac{1}{3} F_{\pi K \to \pi K}^{I_u=(1/2)}(u, t, s) \right]. \qquad (B17)$$

The complete amplitude for the $\pi K \to \pi K$ amplitude is given by

$$t_{\pi K \to \pi K}(s) = \begin{cases} t_{11}^{K\,\text{matrix}}(s) & s < s_{\text{low}} \\ t_{\pi K \to \pi K}^{\text{Regge}}(s) & s > s_{\text{high}} \end{cases}, \qquad (B18)$$

where we choose $\sqrt{s_{\text{low}}} = 2.3$ GeV, $\sqrt{s_{\text{high}}} = 2.5$ GeV for the real part of the amplitude and $\sqrt{s_{\text{high}}} = 2.7$ GeV for the imaginary part of the amplitude as shown in Fig. 12. From the P-wave projection of the Regge amplitude we find the following asymptotic behavior for the phase $\phi_{11}(s)$ and denominator function of the complete amplitudes,

$$\phi_{11} \to \arctan\left[-\frac{\sin\pi\alpha_P(0)}{1 + \cos\pi\alpha_P(0)}\right] = \frac{\pi}{2},$$
$$\frac{1}{D_{\pi K \to \pi K}(s)} \to \frac{i}{s(1/2)}. \tag{B19}$$

The phase is shown in Fig. 12.

[1] B. Diekmann, Phys. Rep. **159**, 99 (1988).
[2] B. Hyams, C. Jones, and P. Weilhammer, Nucl. Phys. **B64**, 134 (1973).
[3] D. Aston *et al.*, Phys. Lett. **92B**, 215 (1980).
[4] D. Bisello *et al.*, Phys. Lett. B **220**, 321 (1989).
[5] A. Donnachie and H. Mirzaie, Z. Phys. C **33**, 407 (1987).
[6] J. J. Dudek, R. G. Edwards, M. J. Peardon, D. G. Richards, and C. E. Thomas, Phys. Rev. D **82**, 034508 (2010).
[7] S. Godfrey and N. Isgur, Phys. Rev. D **32**, 189 (1985).
[8] K. Nakamura *et al.* (Particle Data Group), J. Phys. G **37**, 075021 (2010).
[9] N. N. Achasov and A. A. Kozhevnikov, Phys. At. Nucl. **60**, 1011 (1997).
[10] N. N. Achasov and A. A. Kozhevnikov, Phys. At. Nucl. **65**, 153 (2002).
[11] P. Guo, R. Mitchell, and A. P. Szczepaniak, Phys. Rev. D **82**, 094002 (2010).
[12] M. Ablikim *et al.* (BES Collaboration), Phys. Rev. Lett. **97**, 142002 (2006).
[13] X. Liu, B. Zhang, L.-L. Shen, and S.-L. Zhu, Phys. Rev. D **75**, 074017 (2007).
[14] B. A. Li, Phys. Rev. D **76**, 094016 (2007).
[15] A. P. Szczepaniak, P. Guo, M. Battaglieri, and R. De Vita, Phys. Rev. D **82**, 036006 (2010).
[16] S. D. Protopopescu *et al.*, Phys. Rev. D **7**, 1279 (1973).
[17] P. Estabrooks and A. D. Martin, Nucl. Phys. **B79**, 301 (1974).
[18] T. N. Pham and T. N. Truong, Phys. Rev. D **16**, 896 (1977).
[19] D. Aston *et al.*, Nucl. Phys. **B296**, 493 (1988).
[20] R. Mercer *et al.*, Nucl. Phys. **B32**, 381 (1971).
[21] P. Estabrooks *et al.*, Nucl. Phys. **B133**, 490 (1978).
[22] L. Castillejo, R. H. Dalitz, and F. J. Dyson Phys. Rev. **101**, 453 (1956).
[23] J. R. Peláez and F. J. Ynduráin, Phys. Rev. D **69**, 114001 (2004).
[24] B. Ananthanarayan, G. Colangelo, J. Gasser, and H. Leutwyler, Phys. Rep. **353**, 207 (2001).
[25] J. R. Peláez and F. J. Ynduráin, Phys. Rev. D **71**, 074016 (2005).
[26] B. Ananthanarayan, P. Büttiker, and B. Moussallam, Eur. Phys. J. C **22**, 133 (2001).